Empowering PGD-based parametric analysis with Optimal Transport

D. Muñoz [a,*], S. Torregrosa [a,b], O. Allix [c], F. Chinesta [d]

[a] PIMM, Arts et Métiers Institute of Technology, 151 Boulevard de l'Hopital, 75013 Paris, France
[b] STELLANTIS, 10 Boulevard de l'Europe, 78300 Poissy, France
[c] Université Paris-Saclay, ENS Paris-Saclay, CentraleSupélec, CNRS, LMPS - Laboratoire deMécanique Paris-Saclay, 91190, Gif-sur-Yvette, France
[d] ESI Chair, PIMM, Arts et Métiers Institute of Technology, 151 Boulevard de l'Hopital, 75013 Paris, France

ARTICLE INFO

Keywords:
PGD
Optimal Transport
PDEs
POD
sPGD

ABSTRACT

The Proper Generalized Decomposition (PGD) is a Model Order Reduction framework that has been proposed to be able to do parametric analysis of physical problems. These parameters may include material properties, boundary conditions, etc. With this framework most of the computation may done in an off-line stage allowing to perform real time simulation in a variety of situations. Nevertheless, this scheme may lose its efficiency where the domain itself is also considered as "a parameter". Optimal transport techniques, on the other hand, have demonstrated exceptional performance in interpolating different types of fields described over geometrical domains with varying shapes. Hence trying allying both techniques is quite natural. The core idea is that PGD handles the parametric solution, while the optimal transport-based methodology transports the solution for a family of domains defined by geometrical parameters such as lengths, radii, thicknesses, etc. In this first attempt the associated methodology is proposed and apply in simple 1D and 2D cases showing interesting performances.

1. Introduction

Nowadays, the creation of models that accurately represent real systems and respond in real-time is essential for a worldwide community of scientists, engineers, and designers. Those models are commonly described employing Partial Differential Equations (PDEs).

Model Order Reduction (MOR) techniques have been proposed to reduce the computational complexity of physical models obtained through physical-based numerical simulations while maintaining their accuracy. MOR techniques encompass a wide range of algorithms, but we focus on those that aim to reduce the computational cost of physical-based numerical simulations. Among them, the Proper Orthogonal Decomposition (POD) method [1,2] aims to decompose the solution field into a set of modes that represent the variation of the solution. The dominant modes, which capture the most energy, are selected as a reduced basis for solving the PDE problem. On the other hand, the Reduced Basis (RB) method [3] is another MOR technique that has gained significant popularity. It constructs a low-dimensional subspace of the high-dimensional solution space. The RB method solves the problem by projecting the solution onto the subspace and representing it as a linear combination of a small number of basis functions. Both POD and RB methods share the same principles of reducing the computational cost of physical-based numerical simulations. However,

* Corresponding author.
E-mail addresses: david.munoz_pellicer@ensam.eu (D. Muñoz), sergio.torregrosa@stellantis.com (S. Torregrosa), olivier.allix@ens-paris-saclay.fr (O. Allix), francisco.chinesta@ensam.eu (F. Chinesta).

they differ in their approach to constructing the reduced basis. POD decomposes the solution field into modes, while RB constructs a subspace directly. Additionally, POD selects dominant modes as the reduced basis, while RB represents the solution as a linear combination of basis functions.

Both RB and POD techniques are widely used today but are linear methods that present limitations in certain situations. Thus, non-linear dimensionality reduction methods have been developed lately to tackle these limitations. Among the most common non-linear dimensionality reduction techniques, we can mention the kernel Principal Component Analysis (kPCA) [4,5]. kPCA extends the classical linear Principal Component Analysis (PCA) [6,7] to non-linear manifolds operating in a high-dimensional space, without the necessity of constructing a mapping, thanks to the use of a kernel trick. In this feature space, now linear, the PCA can operate. Another important method is the so-called Locally Linear Embedding (LLE) [8,9] which assumes that the data lies on a low-dimensional manifold that can be locally approximated by a linear map. This algorithm tries to find the low-dimensional representation by preserving the local relationship established through vicinities of points.

While many of the aforementioned non-linear methods provide the sought low-dimensional manifold, only a few provide a mapping from the low-dimensional to the original high-dimensional manifold. This characteristic is crucial in reduced-order modeling PDEs. Deep learning [10] strategies such as Auto-encoders [11–13], convolutional auto-encoders [14], and deep convolutional generative adversarial networks [15] have shown promising results in reducing the dimensionality of PDEs. However, aforementioned linear strategies such as POD are still often preferred over deep neural network-based methodologies since they provide an interpretable framework for the analysis of the system, as well as the ability to control the reduced system.

The technologies discussed so far require the construction of a reliable database to construct its latent space, which can subsequently be used to solve PDEs in this new setting. Other technologies rely on the decomposition of the PDE solution into a set of modes that construct a basis of reduced dimensionality compared with the original solution space. Among the methods that fall into this category, the Proper Generalized Decomposition (PGD) [16–18] stands out, and it is the focus of this work. The PGD is based on the separability of the solution into a set of bases or modes, enabling the direct consideration of parametric problems in the formulation of the equations. The approximation is successively enriched by adding more modes. Unlike POD, the PGD modes are not orthogonal to each other. The PGD approach can handle various extra coordinates, including source terms, boundary conditions, initial conditions, and material properties, among others. The resulting model has an increased dimensionality compared to the original solution space, as it includes the standard physical coordinates (space and time) plus all the extra coordinates introduced. Despite this, the PGD framework allows for easy inverse identification or optimization in the *a posteriori* stage. This framework also enables efficient calculations since the envelope containing all possible solutions has been pre-calculated offline in the form of a parametric solution expressed in a separated form that circumvents the curse of dimensionality. This opens new possibilities for simulation-based real-time control, where the pre-calculated parametric solution can be used as a transfer function for online control and augmented reality with light computing platforms such as tablets or smartphones.

However, the PGD framework may not directly consider parameters related to the geometrical domain where the solution is sought. This issue has been addressed in [19], where different mappings between domains are considered to alleviate this obstacle. Nevertheless, in this paper, we consider a more generic approach which do not require, a priori, a domain decomposition framework. The proposed methodology uses techniques from the field of Optimal Transport (OT) to interpolate the parametric solutions, derived from the PGD, between two or more parameterized geometrical domains. Most common interpolation techniques are discarded since they may introduce artifacts or make difficult interpolation. The OT-based methodology efficiently transports the solution to new spatial domains defined by geometrical parameters such as lengths, radii, thicknesses, etc., respecting the response in real-time. This combination of PGD and OT techniques allows for accurate and efficient modeling of physical systems in complex geometries.

2. Optimal Transport overview

Optimal Transport [20] is a mathematical framework that addresses the problem of how to transport mass or resources from one location to another in an optimal way. The Optimal Transport problem has several important applications in machine learning, including generative modeling, domain adaptation, and data alignment. It has also been used in image processing, computer vision, and optimal control. The concept of optimal transport is well-defined within its specific application domain. However, the focus of this paper is to extend and apply this idea to PGD modes, which necessitates several simplifications. The problem of optimal transport has its roots in the works of Monge [21] and Kantorovich [22], who introduced the problem in the context of economics and applied mathematics. A modern formulation of the problem can be found in the book of Villani [23], who showed the connection between optimal transport and a wide range of fields.

The Optimal Transport problem can be mathematically formulated considering two probability measures μ and ν defined on two metric spaces X and Y respectively. The goal is to find a transportation plan $\hat{\gamma}$ that minimizes the cost function given by Eq. (1):

$$\gamma = \inf_{\hat{\gamma} \in \Pi(\mu,\nu)} \int_{X \times Y} c(x,y) d\hat{\gamma}(x,y), \tag{1}$$

where $\Pi(\mu,\nu)$ denotes the set of all joint probability measures on $X \times Y$ with marginals μ and ν, and $c(x,y)$ is the cost of transporting a unit of mass from x to y. In other words, γ is a measure on $X \times Y$ that assigns a mass $\gamma(x,y)$ to each pair (x,y) such that the total mass transported from X to Y is equal to μ and ν.

One of the key developments in the field of Optimal Transport is the Wasserstein distance [24]. This distance measure is derived from the optimal transport problem and has been shown to be useful in various applications such as image matching, clustering, and shape analysis. Computing the Wasserstein metric directly between two PGD modes is not possible since these modes are not

probability measures. This challenge has been addressed in previous works [25,26]. One possible approach is to decompose each PGD mode into positive and negative components.

Recently, there has been growing interest in the use of entropic regularization of optimal transport, which introduces a regularization term into the cost function. This approach has been shown to have important applications in machine learning, particularly in the area of generative modeling [27–29].

As mentioned before, our objective is to utilize optimal transport to transfer PGD modes from two or more geometrical domains into a new intermediate domain. To simplify the problem and align with our current context, we adopt a discrete version of optimal transport, which better suits our needs. Using a particle-based decomposition strategy, our aim is to accurately approximate these modes and convert the cost minimization problem into a more manageable assignment problem. We specifically address Monge's original problem from a discrete perspective. Our goal is to find the optimal method for transporting particles from one distribution to another, with the objective of minimizing the square of the Euclidean distance traveled. Let us consider two distributions of particles. The first distribution consists of N particles, each characterized by a mass a_n and a location x_n. The second distribution comprises M particles, each with a mass b_m and a location y_m. In order to solve this problem, we enforce the constraint of mass conservation. To formalize this, we introduce the concepts of measure: the origin distribution is denoted as α, and the target distribution is denoted as β,

$$\alpha = \sum_{n=1}^{N} a_n \delta_{x_n}(x) \quad \text{and} \quad \beta = \sum_{m=1}^{M} b_m \delta_{y_m}(y), \tag{2}$$

where $\delta_{x_n}(x)$ and $\delta_{y_m}(y)$ are the Dirac delta distributions at position x_n and y_n, respectively.

As in Eq. (1), the problem consists in looking for the transport map γ that connect each point x_n with a single point y_m such it pushes the origin mass α to the target mass β. As no matter can be produced or destroyed during the transport, the map γ must satisfy the mass conservation,

$$b_m = \sum_{n:\gamma(x_n)=y_m} a_n \quad | \quad \forall m \in \{1, \dots, m, \dots, M\} \tag{3}$$

Additionally, this map must minimize the transportation cost which is defined as the square of the Euclidean distance between the origin particle n and the target particle m:

$$C(x_n, y_m) = \|x_n - y_m\|^2, \tag{4}$$

Then, the simplified optimal transport problem may become:

$$\gamma = \min_{\hat{\gamma}} \sum_{n=1}^{N} C(x_n, \hat{\gamma}(x_n)). \tag{5}$$

We can further simplify this problem by assuming an equal number of particles, denoted as $N = M$. Additionally, we assume that each particle has the same mass, represented as $a_n = \frac{1}{N}$, and that each target location receives an equal amount of mass, denoted as $b_m = a_n$. Consequently, the minimization problem stated in Eq. (5) can be transformed into a deterministic assignment problem [30].

Under these hypotheses, the 1D problem, equivalent to the assignment problem represents the simplest optimal transport problem. Indeed, in this case, the solution simply consists in sorting the particles' locations along the 1D axis in ascending order. Then, one can match the first origin position with the first target position and this successively. In 2D, this same problem gets more complicated since no order relation holds, but the problem remains easy to solve. Indeed, the problem consists of the optimal assignment problem between two point clouds. Each cloud has the same number of points and each point has the same amount of mass. In higher dimensions, the problem is not more complicated but the computational cost is increased due to the calculation of the distances. This does not hold when more than two clouds are considered, where the problem cannot be solved through assignment techniques and must be addressed with other methods.

Once two point clouds are optimally matched, it is possible to interpolate between them, in an optimal transport way. All the points from the source distribution may be partially displaced along the corresponding segment created between each point of the source distribution and the corresponding optimal match on the target distribution.

3. OT-PGD

The construction of the parametric model represents the offline stage of the methodology and consists of four steps. First, we gather the different parametric PGD solutions, each of them associated to one set of geometrical parameters. Then, each spatial mode of the solution is decomposed into a set of Gaussian functions whose sum equals the original mode. After the Gaussian decomposition, we continue with its optimal matching. This step consists in pairing each Gaussian from each mode in each parametric solution with one, and only one, Gaussian from the respective mode in the rest of the solutions. This step is computed through a Genetic algorithm that minimizes the optimal transport cost, which is, as seen above, the cost of transporting each particle. At this stage the reduced model regarding the geometrical parameter remain to be constructed. To achieve this final step we proceed as follows. A POD is applied to the snapshots representing the location of the Gaussian functions in each parametric solution. Finally, a regression model is trained over the retained POD coefficients, leading to the parametric model. This model can be assessed in an online manner to explore the whole space of the geometric parameters, retaining as well the PGD parametric solution [31].

3.1. Reference problem

To show the methodology proposed we lean on the following reference problem. This problem consists of the 1D steady heat equation whose thermal diffusivity is parameterized regarding the standard PGD framework. The geometrical parameters, in this case, describe the length of the spatial domain and will be taken care of by the methodology proposed. Eq. (6) represents the aforementioned problem:

$$\begin{cases} \kappa \dfrac{\partial^2 T(x)}{\partial x^2} = f(x) \quad \forall x \in \Omega_x \\ T(x) = 0 \quad \forall x \in \Gamma_D, \end{cases} \tag{6}$$

where $T(x)$ is the temperature field, κ is the thermal diffusivity of the domain, $f(x)$ is the source term which is defined as $f(x) = G_{\sigma,\mu}(x) = \frac{1}{\sigma\sqrt{2\pi}} e^{\frac{-(x-\mu)^2}{2\sigma}}$ and Γ_D is introduced as the boundary with imposed Dirichlet conditions, in this case, both ends.

The PGD framework allows solving the heat equation only once for any value of the thermal diffusivity in a given range, thus providing a sort of abacus or parametric solution. To compute this parametric solution, however, the diffusivity is an extra coordinate of the problem. So, as we solve the steady behavior of the problem, this is then defined for $(x, \kappa) \in \Omega_x \times \Omega_\kappa$, with $\Omega_x \subset \mathbb{R}$ and $\Omega_\kappa \subset \mathbb{R}$.

Thus, instead of solving a series of diffusion problems for different discrete values of the thermal diffusivity parameter, we wish to solve at once a more general problem. This is not a major issue for the PGD, whose computation complexity scales only linearly with the problem dimensions because of the separated representation considered.

The procedure to solve the parametric problem is defined below. Starting from the weighted residual form of (6), which reads:

$$\int_{\Omega_x \times \Omega_\kappa} T^* \cdot (\kappa \frac{\partial^2 T}{\partial x^2} - f) \cdot dx \cdot d\kappa = 0, \tag{7}$$

for all suitable test functions T^*.

The PGD-separated approximation of the general solution would then be of the form:

$$T(x,k) = \sum_{i=1}^{M} X_i(x) \cdot Z_i(k), \tag{8}$$

wherein the unknown functions $Z_i(\kappa)$ are defined in the domain Ω_κ of values for the thermal diffusivity, while the unknown functions $X_i(x)$ are defined in the spatial domain Ω_x. The M corresponds with the total of PGD modes used to approximate the solution.

Each term of the expansion is computed one at a time, thus enriching the PGD solution until a suitable convergence criterion is satisfied. At enrichment step n of the PGD algorithm, the following approximation is already known,

$$T^{n-1}(x,k) = \sum_{i=1}^{n-1} X_i(x) \cdot Z_i(k). \tag{9}$$

We wish to compute the next functional product $X_n(x) \cdot Z_n(k)$, which we write as $R(x) \cdot W(k)$ to avoid confusion with the already calculated modes.

Thus, the solution at enrichment step n reads

$$T(x,k) = T^{n-1}(x,k) + R(x) \cdot W(k). \tag{10}$$

The weighted residual form (7) yields a non-linear problem for the unknown functions R and W, which we solve iteratively employing an alternating direction scheme until a fixed point is reached.

Following this rationale, we solve the parametric problem described in (6) regarding two different geometrical domains. For the first one, the spatial domain is $\Omega_x^1 = (-1, 1)$ and the parametric domain $\Omega_\kappa^1 = (1, 2)$ with a source term $f^1(x) = G_{\sigma_1,\mu_1}(x)$, where $\sigma_1 = 0.025$ and $\mu_1 = -0.5$. While for the second one, the spatial domain is $\Omega_x^2 = (-3, 3)$ and the parametric domain $\Omega_\kappa^2 = (1, 2)$ with a source term $f^2(x) = G_{\sigma_2,\mu_2}(x)$, where $\sigma_2 = 0.025$ and $\mu_2 = -1.5$. Fig. 1 shows the parametric solution for the two problems considering three different values of thermal diffusivity.

Particle decomposition. Leaning on the reference problem, the Design of Experiments (DoE) consists of two parametric solutions with different geometrical parameters, in particular, the lengths of the spatial domain. Each solution is composed of a set of modes, regarding the reference problems, those modes are defined over the spatial domain and over the parametric domain, i.e. the thermal diffusivity. We consider that the parametric modes are a set of weights that may be directly interpolated for the different lengths of the spatial domains, whereas the spatial modes cannot be directly interpolated. For those modes, we apply the techniques coming from the optimal transport. Therefore, for the $ith-$ spatial mode X_i^g, where g represents the current geometrical domain, we must discretize it employing a sum of Gaussian functions. Following the Smoothed-Particle Hydrodynamics (SPH) [32,33] rationale, each function is associated with a particle located in the spatial domain. This procedure starts by normalizing the spatial modes as,

$$\hat{X}_i^g = \frac{X_i^g}{I_i^g} \qquad \text{where} \qquad I_i^g = \int_{\Omega_x^g} X_i^g \, d\Omega_x^g \tag{11}$$

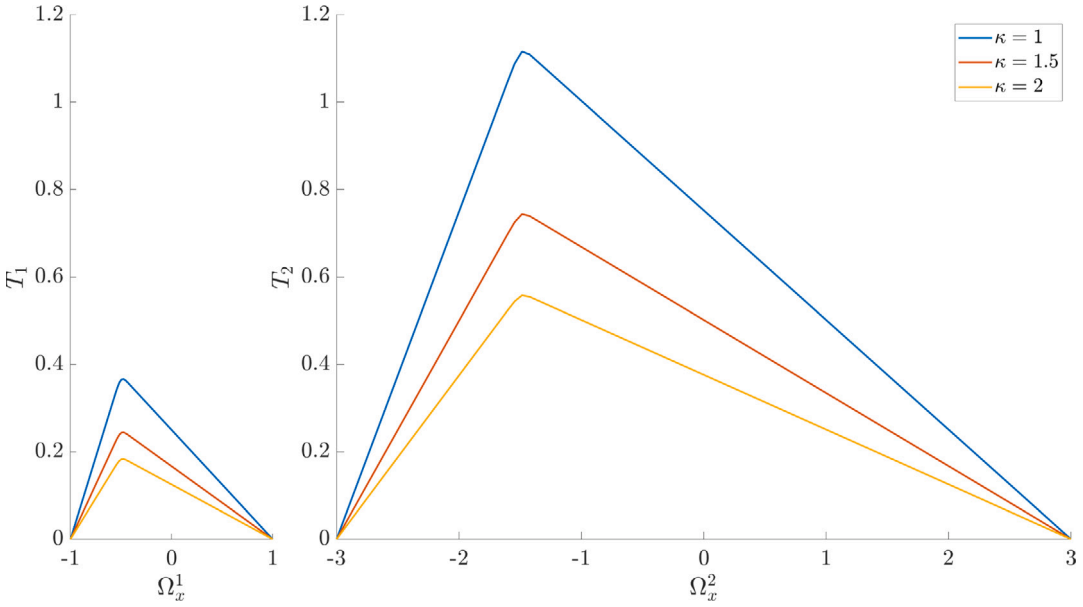

Fig. 1. Reference problem: *Vademecum* of solutions in each geometrical domain. These curves represent the temperature field in each domain particularized for the values of $\kappa = 1$ (in blue), $\kappa = 1.5$ (in orange) and $\kappa = 2$ (in yellow).

The particle-based decomposition allows converting any function into a sum of particles, each of them associated with a Gaussian distribution. In particular, we employ this technique to reconstruct each mode of the PGD, then this functions is defined as:

$$\rho_i^g(x) = \sum_{n=1}^{N} G_{\mu_{i,n}^g,\sigma}(x) \qquad \text{where} \qquad G_{\mu_n^g,\sigma}(x) = \frac{1}{N\sigma\sqrt{2\pi}} e^{\frac{-(x-\mu_n)^2}{2\sigma^2}}, \tag{12}$$

Without loss of generality we set the value of σ constant and the same for each Gaussian function as a hyperparameter. Then, the only variables per distribution are the means μ_i^g of the Gaussian functions, which represent the position of the particle in the spatial domain. The value of μ_i^g is the result of an optimization problem that tries to minimize the discrepancy between the normalized spatial $ith-$PGD-mode $\hat{X}_i^g$ and its corresponding particle decomposition ρ_i^g as,

$$\min_{\mu_i^g} \frac{1}{2} \left[\sum_{i=1}^{D} \left(\hat{X}_i^g(x_i) - \rho_i^g(x_i) \right)^2 \right], \tag{13}$$

where x_i is a sampling point in Ω_x^g and D is the number of sampling points, not necessarily corresponding to the nodes of the mesh or the position of the particles. The optimization problem may be addressed by any algorithm, but in this case, we propose the use of gradient-based optimization algorithms as the expression of the gradient is available, thus its calculation is not costly.

Fig. 2 shows the first PGD mode (in black) compared with the reconstruction achieved with the particle decomposition (in blue).

Particle matching. Once the distributions are properly decomposed into N particles, the following step is to match the particle optimally, i.e. minimization of the transportation cost. Regarding the reference problem, this can be seen as an optimal assignment problem between two point clouds, where each point is a particle identified by its coordinates (μ_i^g). Several algorithms have been developed to solve this problem, such as linear programming. We may mention that in 1D the assignment is trivial, just the sorting of the particles is needed. Then, it is possible to interpolate between two distributions by partially displacing all the particles over the corresponding segments built between each particle from one distribution to the other, as illustrated in Fig. 3.

Parametric model. Finally, once the particles of each geometrical domain are optimally matched, we built the parametric model. For the reference problem, this parametric model consists directly of the weighted interpolation between the coordinates of the matched particles from the two distributions. Thus, the location of the particles describing the solution in an intermediate spatial domain $\Omega_x^{1-2} = (-2, 2)$ is illustrated in Fig. 4.

In this case, a transported mode can be described using the geometric parameter, namely the length of the domain denoted as L^g. It is calculated as the difference between the maximum and minimum values of Ω_x^g, expressed as $L^g = \max(\Omega_x^g) - \min(\Omega_x^g)$,

$$\mu_i^{\hat{g}} = \left(1 - \frac{L^{\hat{g}} - L^1}{L^2 - L^1}\right) \cdot \mu_i^1 + \frac{L^{\hat{g}} - L^1}{L^2 - L^1} \cdot \mu_i^2. \tag{14}$$

Once we are able to recover the position of the particles for any value of the geometrical parameters, the PGD modes can be recovered as well. For the reference problem, we consider a new set of geometrical parameters that define the domain as

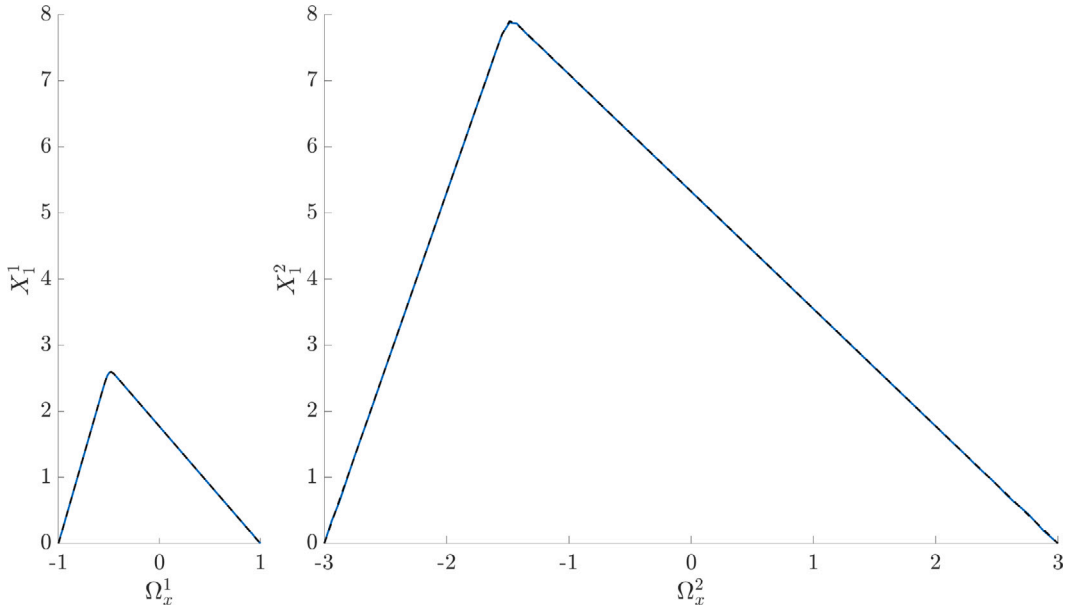

Fig. 2. Reference problem: Particle-based reconstruction of the first PGD mode (in blue) and the corresponding PGD reference mode (in black).

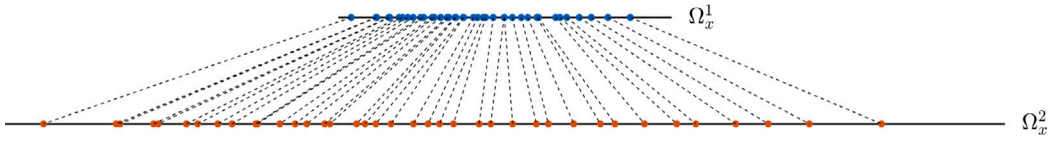

Fig. 3. Reference problem: Optimal matching of the particles in each distribution, one per geometrical domain.

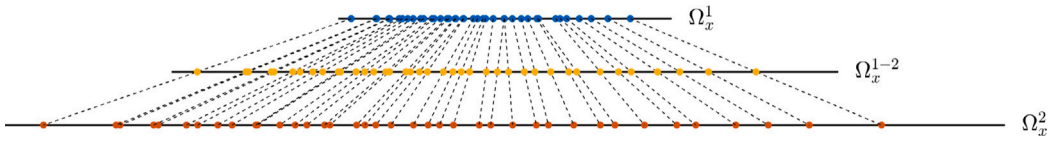

Fig. 4. Reference problem: New set of particles for the domain Ω_x^{1-2}. This particles are obtained by partially displacing all the particles over the corresponding segments.

$\Omega_x^{1-2} = (-2, 2)$. By partially displacing the particles over the assignment segments we are able to obtain the corresponding position of the particles. Following the expression (12), we add the contribution of each particle and then multiply by the total mass I, which is interpolated as well. This procedure gives as a result the recovered PGD mode X_1^{1-2} represented in Fig. 5.

The previous strategy should be repeated for each of the spatial modes composing the parametric PGD solution. With the combination of each interpolated PGD mode, we can recompose the parametric solution into the new geometrical domain (Ω_x^{1-2}), as illustrated in Fig. 6.

3.1.1. Parametric boundary condition problem

In order to illustrate the functionality of this methodology in capturing multiple PGD modes, we present the following problem, which again relies on the 1D heat equation. In this scenario, the additional parameter is the source term ($f(x)$ in Eq. (6)). The source term is represented by a Gaussian function given by $f(x) = G_\sigma(x, f_\mu) = \frac{1}{\sigma\sqrt{2\pi}} e^{-(x-f_\mu)^2/2\sigma}$, where the mean value f_μ is considered as the extra-coordinate within the PGD framework, and the standard deviation σ is specified for each problem. Similar to the reference problem, we define two spatial domains: the first domain is described by $\Omega_x^1 = (-1, 1)$, while the second domain is described by $\Omega_x^2 = (-3, 3)$. Within the PGD framework, the extra-coordinates that define the source terms are defined over $\Omega_{f_\mu}^1 = (-0.5, 0.5)$ and $\Omega_{f_\mu}^2 = (-1.5, 1.5)$, respectively. Finally, the remaining constants are set as follows: $\sigma_1 = 0.1$, $\sigma_2 = 0.3$, and $\kappa_1 = \kappa_2 = 1$.

With a well-defined problem in place, we utilize the PGD solver to obtain the set of modes. Specifically, a set of 10 modes adequately captures the characteristics of the parametric solution. The resulting particular solutions for three different values of f_μ in each domain, using these 10 modes, are depicted in Fig. 7.

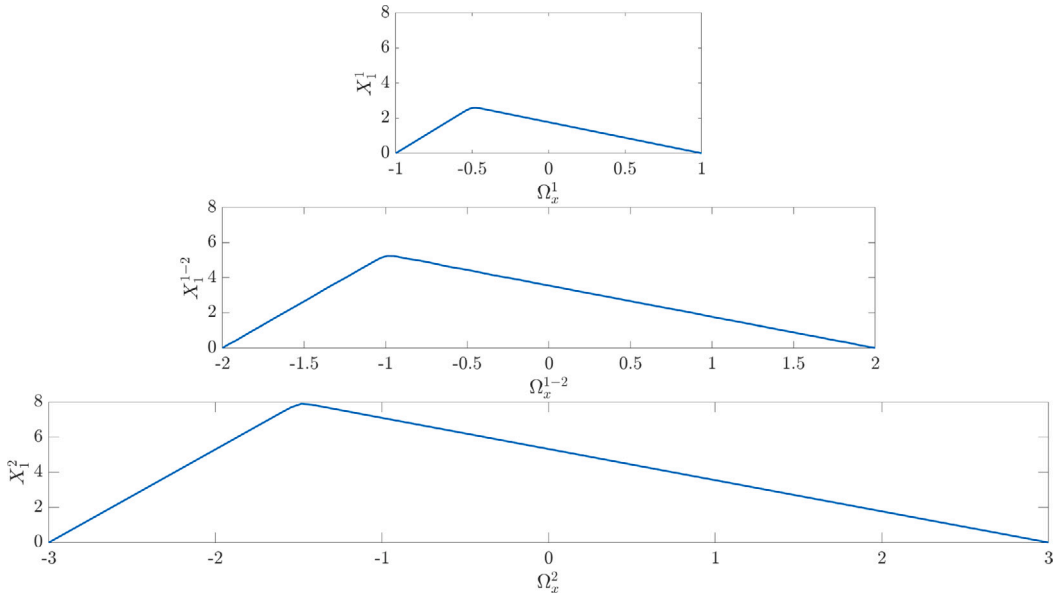

Fig. 5. Reference problem: Transported PGD mode to the domain Ω_x^{1-2}.

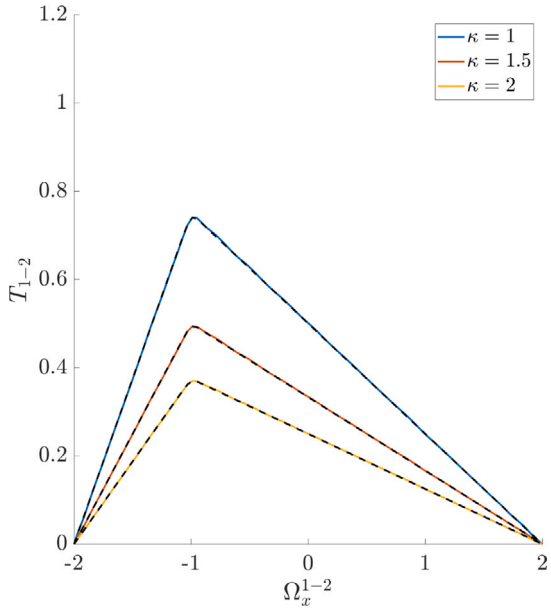

Fig. 6. Reference problem: Parametric solutions transported to the domain Ω_x^{1-2}. The temperature field is particularized for three values of κ: 1 (in blue), 1.5 (in orange) and 2 (in yellow). Additionally, the reference solution is represented for each value of κ (in black).

Particle decomposition. The subsequent stage, following the aforementioned methodology, involves the particle-based representation. While this step is performed for each of the 10 PGD modes constituting the parametric solution, the first three modes are depicted in Fig. 8. Specifically, this figure exhibits the reference PGD mode (shown in black) and its corresponding particle-based reconstruction within each geometric domain.

It is important to highlight that certain regions within the modes may exhibit negative values. To effectively tackle this issue, we propose a strategy that entails dividing the original domain into multiple subdomains based on the sign of the values. The subsequent process follows the usual procedure for each of these subdomains. This strategy is depicted in Fig. 9. It is worth noting

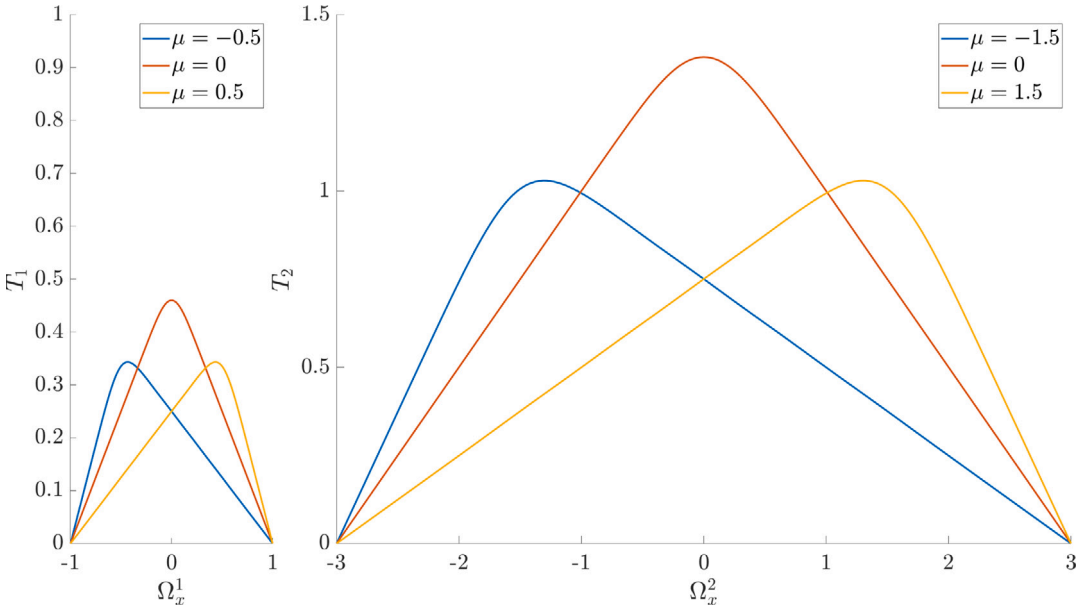

Fig. 7. *Vademecum* of solutions for the temperature field for the parameterized boundary conditions problem. On the left, three particular solution of the temperature field over the domain Ω_x^1 corresponding to the values of $f_\mu = -0.5$ (in blue), $f_\mu = 0$ (in orange) and $f_\mu = 0.5$ (in yellow). On the right, three particular solution of the temperature field over the domain Ω_x^2 corresponding to the values of $f_\mu = -1.5$ (in blue), $f_\mu = 0$ (in orange) and $f_\mu = 1.5$ (in yellow).

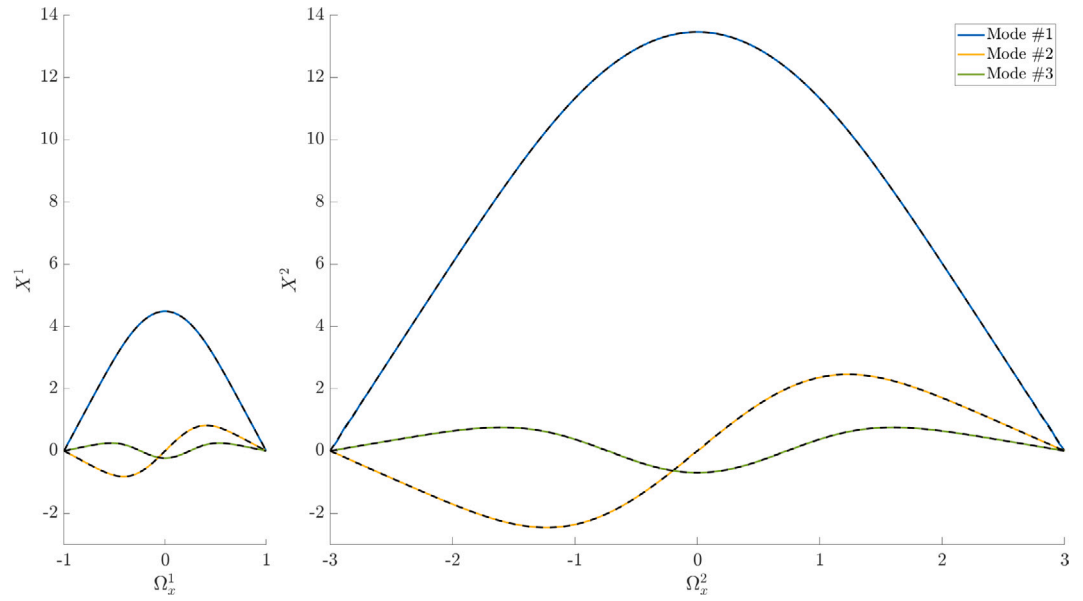

Fig. 8. Particle-based decomposition of the first three PGD modes, along with the reference ones (in black).

that within subdomains where the mode takes negative values, these values are considered in absolute terms, represented by the dashed line in the Figure.

Particle matching. The methodology proceeds with the matching of the two distributions for each PGD mode, considering the problem's involvement of a single spatial dimension and two distributions. The optimal matching solution can be obtained by sorting the particles that represent each PGD mode. Fig. 10 illustrates the matching of the two geometric domains for the third PGD mode, where the particles are categorized based on their recovery of the positive or negative part of the PGD mode.

Parametric model. The parametric model used to displace particles and generate additional solutions is obtained through weighted linear interpolation. This model moves the particles along the segments formed during the matching stage following the expression

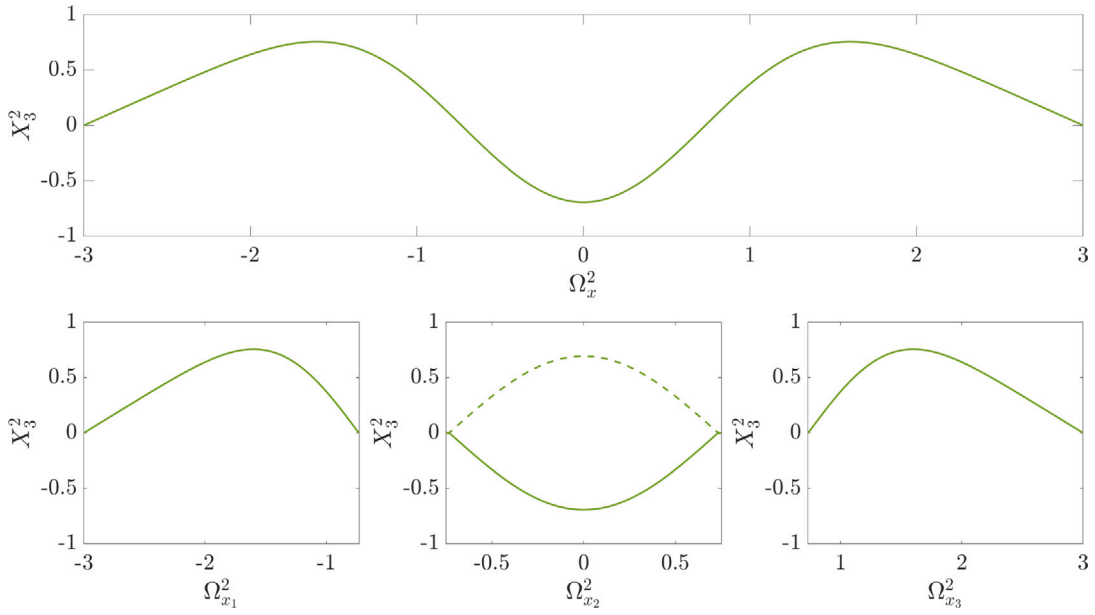

Fig. 9. Representation of the subdivision of the third mode of the domain Ω_x^2 into subdomains.

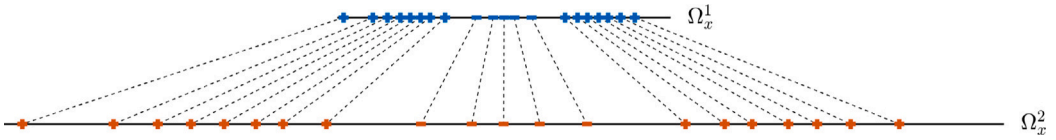

Fig. 10. Visual representation showcasing the optimal alignment of particles within each geometrical domain. The symbols indicate the particles belonging to the positive and negative regions.

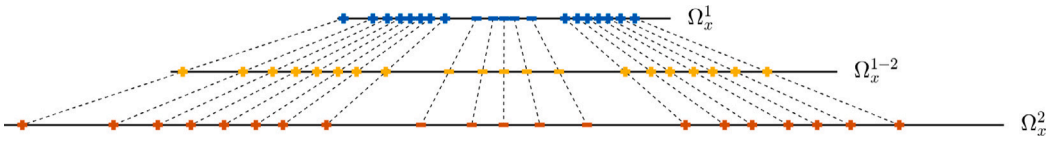

Fig. 11. Representation of the new set of particles that describe the third PGD mode for the domain Ω_x^{1-2}.

in Eq. (14). Fig. 11 shows the position of the particles for a new geometrical domain described as $\Omega_x^{1-2} = (-2, 2)$. It is important to note that the status of a transported particle, whether it is positive or negative, depends on the status of the particles used to transport it. If both particles are positive, the resulting particle will also be positive, and vice versa.

Fig. 12 illustrates the procedure the parametric model follows, where the positions of particles from the first three modes in two reference geometrical domains are used to compute the same modes in a different domain.

When this procedure is repeated for the 10 modes, the parametric solution can be reconstructed for any intermediate geometry. Depending on the value of the load position, each mode is weighted by the extra-coordinate mode. By adding all contributions, we obtain a set of solutions as shown in Fig. 13.

3.2. Parametric 2D problem

The following example aims at showing how this methodology behaves when more than one spatial dimensions are involved in the problem. The equation to be addressed is, as in the reference example, the heat equation whose thermal diffusivity is parameterized through the PGD framework over a 2D spatial domain,

$$\begin{cases} \kappa \Delta T(x, y) = f(x, y) \quad \forall (x, y) \in \Omega_{x,y} \\ T(x, y) = 0 \quad \forall (x, y) \in \Gamma_D, \end{cases} \tag{15}$$

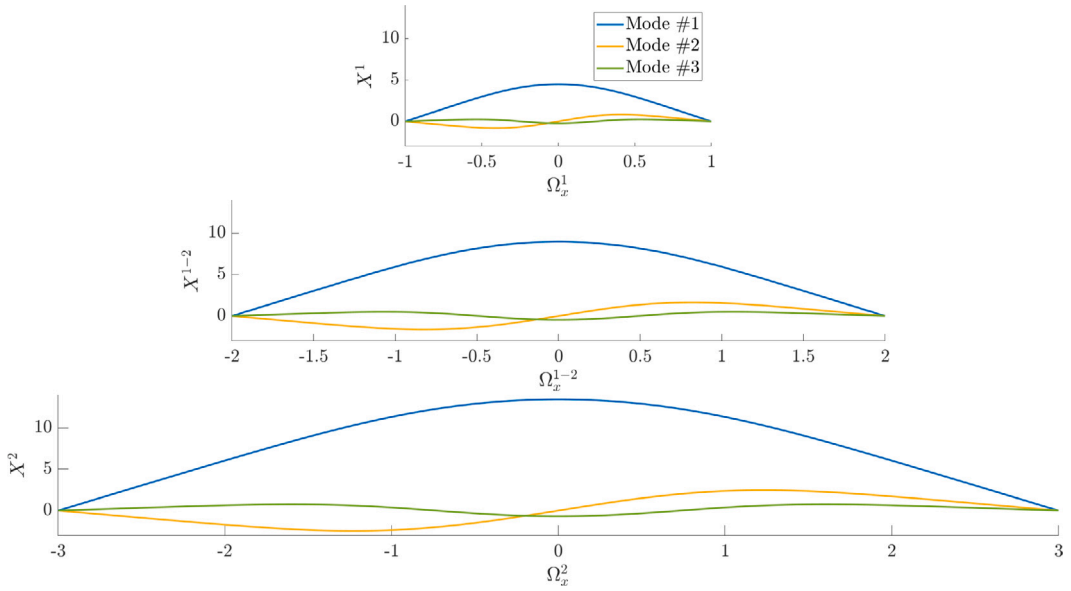

Fig. 12. Transportation of the three first PGD modes into the domain Ω_x^{1-2}.

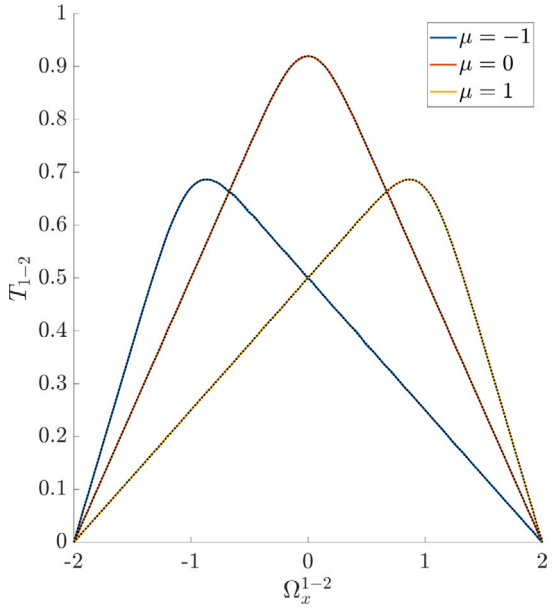

Fig. 13. Transported *vademecum* of solutions. Three particular solutions of the temperature field are represented for the values of $f_\mu = -1$ (in blue), $f_\mu = 0$ (in orange) and $f_\mu = 1$ (in yellow). Also, the reference solution is shown in black.

Let κ represent the thermal diffusivity, which is considered an extra coordinate for the PGD (Proper Generalized Decomposition) defined over $\Omega_\kappa = (1, 2)$. Consequently, Ω_κ extends the problem domain. The temperature field, denoted by T, is defined to be 0 over the Dirichlet boundaries Γ_D. The source term, $f(x, y)$, is characterized by a bivariate Gaussian function, i.e., $f(x, y) = G_{[\mu_x,\mu_y],[\sigma_x,\sigma_y]} = \frac{1}{\sigma_x\sigma_y 2\pi} e^{-[(x-\mu_x)^2/2\sigma_x + (y-\mu_y)^2/2\sigma_y]}$. As previously mentioned, the 2D space $\Omega_{x,y}$ is defined such that each geometric domain corresponds to an ellipse described by the lengths of its semi-axes: a horizontal axis l_h and a vertical axis l_v. Therefore, $\Omega_{x,y} = (l_h, l_v)$.

Fig. 14 illustrates four geometrical domains utilized for exploring the geometric parameter space, namely the horizontal and vertical semi-axes, denoted as $\Omega^1_{x,y} = (1, 1)$, $\Omega^2_{x,y} = (1, 1.5)$, $\Omega^3_{x,y} = (3, 1)$, and $\Omega^4_{x,y} = (3, 1.5)$. Each domain represents a specific solution of the temperature field within the entire parametric range, with a thermal diffusivity value of $\kappa = 1$. The corresponding source terms for each solution are defined as $G^1_{[0,0],[0.5,0.5]}$, $G^2_{[0,0],[0.5,0.75]}$, $G^3_{[0,0],[1.5,0.5]}$, and $G^4_{[0,0],[1.5,0.75]}$.

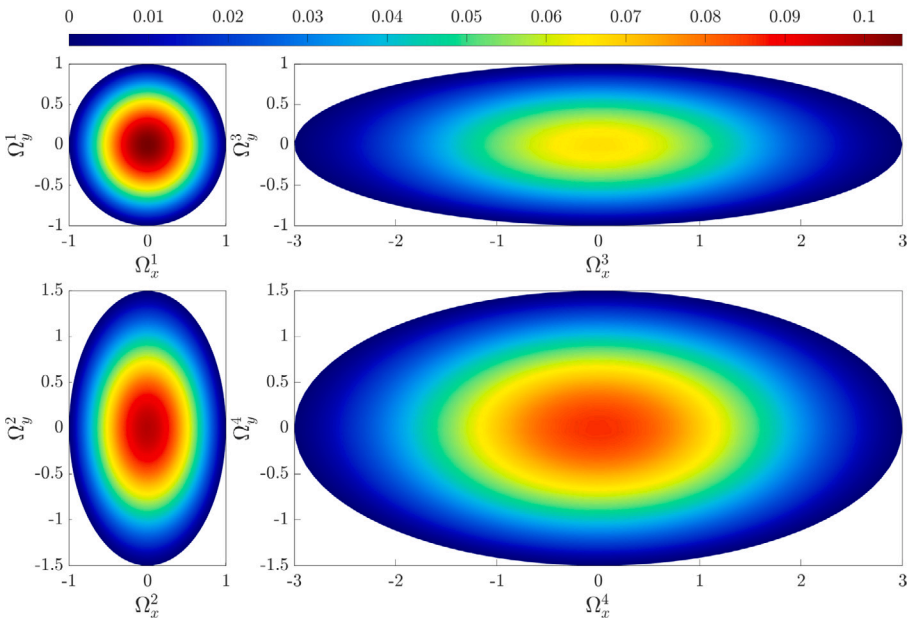

Fig. 14. Sampling of the space of geometrical parameters that contains four individuals. Each spatial domain is illustrated with its corresponding temperature field considering a value of $\kappa = 1$.

Particle decomposition. Regarding the particle decomposition of each PGD mode, it is worth noting that although each particle is now located within a 2D spatial domain, the methodology for the 1D problem remains applicable. In this context, the particle-based decomposition employs the following function to reconstruct each PGD mode,

$$\rho_i^g(x,y) = \sum_{n=1}^{N} G_{[\mu_{i,n_x}^g,\mu_{i,n_y}^g],[\sigma_{i,x},\sigma_{i,y}]}(x,y) \quad \text{where} \quad G_{[\mu_x,\mu_y],[\sigma_x,\sigma_y]}(x,y) = \frac{1}{N\sigma_x\sigma_y 2\pi} e^{-\left[(x-\mu_x)^2/2\sigma_x + (y-\mu_y)^2/2\sigma_y\right]}, \tag{16}$$

With the same rational, the minimization problem presented through Eq. (5) must be modified to consider the additional dimension of the particles as follows:

$$\min_{\mu_i^g} \frac{1}{2}\left[\sum_{i=1}^{D}\left(\widehat{X}_i^g(x_i,y_i) - \rho_i^g(x_i,y_i)\right)^2\right], \tag{17}$$

being μ_i^g a matrix that contains the coordinates x and y of each particle in the distribution, which may be formalized as follows:

$$\mu_i^g = \left[[\mu_{i,1_x}^g, \mu_{i,1_y}^g] \quad \cdots \quad [\mu_{i,n_x}^g, \mu_{i,n_y}^g] \quad \cdots \quad [\mu_{i,N_x}^g, \mu_{i,N_y}^g]\right]^T \in \mathbb{R}^{N\times 2}. \tag{18}$$

Particle matching. In accordance with the methodology, the subsequent step involves optimal matching. However, the complexity increases when attempting to interpolate between multiple distributions defined over multiple dimensions. In fact, the matching process must be performed between each distribution and every other distribution. Consequently, each particle within a distribution needs to be paired with one, and only one, particle from each of the other distributions, minimizing the cost of transporting the particle.

Therefore, one can introduce $\mu_i^g \in \mathbb{R}^{N\times d}$, as the matrix composed by the coordinates of every particle of the PGD mode i in the geometry g. Hence, the cost between two distributions g and g' is defined as the sum of the square of the Euclidean distances between the paired particles in each distribution:

$$C_{i,[g,g']}(\phi_g,\phi_{g'}) = \sum_{n=1}^{N}\left\|\mu_{i,\phi_g(n)}^g - \mu_{i,\phi_{g'}(n)}^{g'}\right\|_2^2, \tag{19}$$

where ϕ_g is a function that permutes the N particles, so it represents the ordering of the particles. One seeks the optimal function, i.e., the ordering that corresponds to the optimal matching to minimize the defined cost. Then, the cost between the G geometries is defined as the sum of the cost between two distributions for all the possible pairs of distributions, i.e., the sum of the cost between all possible pairs:

$$\boldsymbol{C}_{i,G}(\phi_1,\ldots,\phi_g,\ldots,\phi_G) = \sum_{g=1}^{G}\sum_{\substack{g'=1,\\ g\neq g'}}^{G} C_{i,[g,g']}(\phi_g,\phi_{g'}). \tag{20}$$

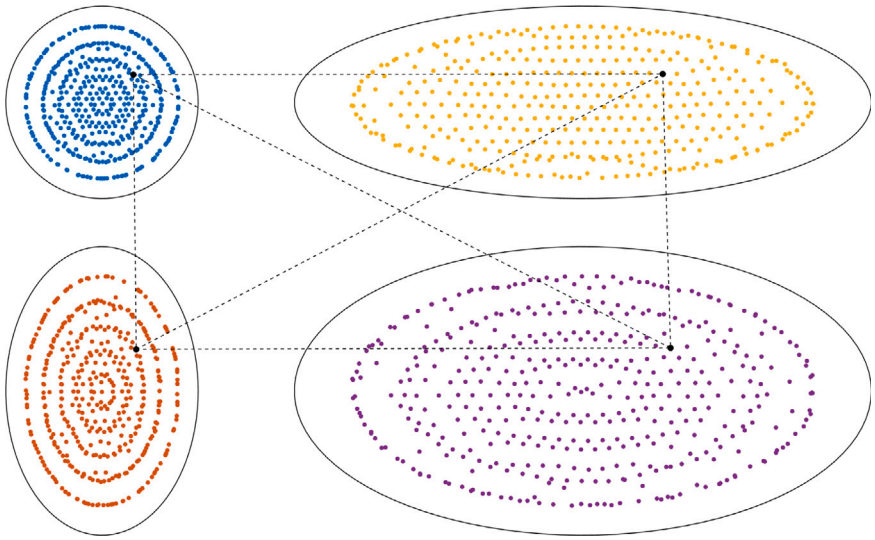

Fig. 15. Particle-based decomposition for each distribution. Also, for one particle, is represented the segments that correspond with the optimal matching.

Thus, the optimal matching problem seeks for the set of orderings $\phi_g \in \{\phi_1, \dots, \phi_g, \dots, \phi_G\}$ that minimize (20). So, the problem reads,

$$\min_{\phi_1,\dots,\phi_g,\dots,\phi_G} \boldsymbol{C}_{i,G}(\phi_1, \dots, \phi_g, \dots, \phi_G). \tag{21}$$

To solve this minimization problem, a Genetic Algorithm (GA) [34–36] is implemented. The resulting assignment performed by the GA algorithm is represented (for one particle) in Fig. 15.

Parametric model. In this example, the complexity is also increased during the construction of the parametric model. The main objective is to establish a mapping that can determine the particle locations for a given set of geometrical parameters. Once this mapping is obtained, we can reconstruct the complete parametric solution. Various algorithms can be employed to achieve this goal, and in the context of regression techniques, we choose the Sparse Proper Generalized Decomposition (sPGD) [37]. This technique utilizes the available information regarding each set of geometrical parameters to determine the particle positions in unexplored regions of the geometrical parameter space. To simplify the calculations, we combine this algorithm with the Proper Orthogonal Decomposition (POD), which is a well-known method for dimensionality reduction in a given problem.

The initial task involves organizing the available information, which pertains to the positions of the particles within each geometrical domain. The matrix μ_i represents the coordinates of each particle across the different geometrical domains, where the subscript i corresponds to the PGD mode:

$$\mu_i = \begin{bmatrix} \mu_i^1(:) & \cdots & \mu_i^g(:) & \cdots & \mu_i^G(:) \end{bmatrix} \in \mathbb{R}^{2N \times P}, \tag{22}$$

where the rows represent the coordinates of each particle and the columns represent the number of geometric domains. To analyze this matrix, we employ POD. The first step of POD involves applying Singular Value Decomposition (SVD) to μ_i. This decomposition yields the following result:

$$\mu_i = U_i \cdot \Sigma_i \cdot V_i^T. \tag{23}$$

The simplification relies in the fact that we retain only the first modes i.e; with the highest singular value. Therefore, the reconstruction of the matrix μ_i, considering a reduced number of POD modes, can be expressed as follows:

$$\mu_i \approx U_{i,r} \cdot \Sigma_{i,r} \cdot V_{i,r}^T = U_{i,r} \cdot \theta_{i,r}. \tag{24}$$

The retained modes $U_{i,r}$ are accompanied by the corresponding coefficients, $\theta_{i,r}$. Having obtained these terms, we proceed to the next step, which involves determining the value of the coefficients $\theta_{i,r}$ for any given set of geometrical parameters. To accomplish this, we employ the sPGD regression technique, which utilizes a separated approximation for each individual geometrical parameter. This approximation can be expressed using the following equation:

$$\theta_{i,r} \approx \hat{\theta}_{i,r} = \sum_{m=1}^{M} \prod_{q=1}^{Q} \psi_{i,m}^q(\alpha_q), \tag{25}$$

where α_q represents the geometrical parameters, in particular the horizontal l_h and vertical l_v semi-axes of the ellipse. Also, ψ_m^q is an univariate function related to the qth geometrical parameter and the mth sPGD mode. Assuming that each dimension q in the

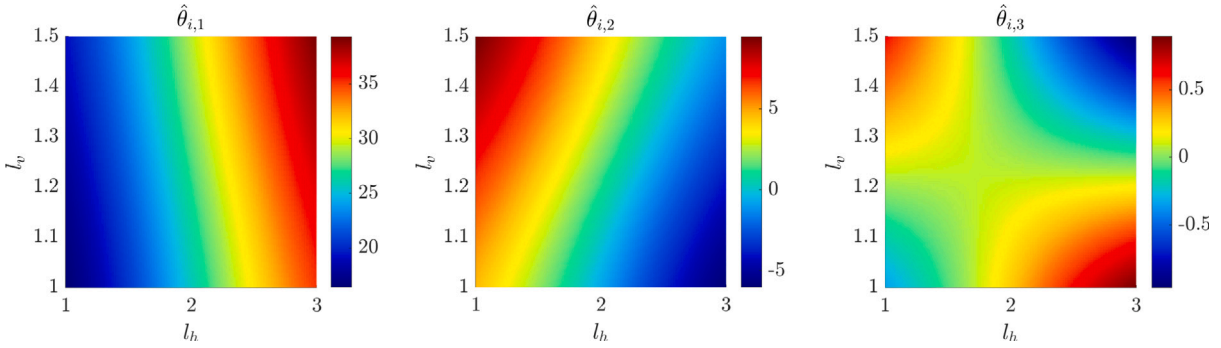

Fig. 16. Reference problem 2D: sPGD regression of the POD coefficients $\hat{\theta}_{i,r1}$, $\hat{\theta}_{i,2}$ and $\hat{\theta}_{i,3}$ for any value of the geometrical parameters $\hat{l}_h$ and $\hat{l}_v$.

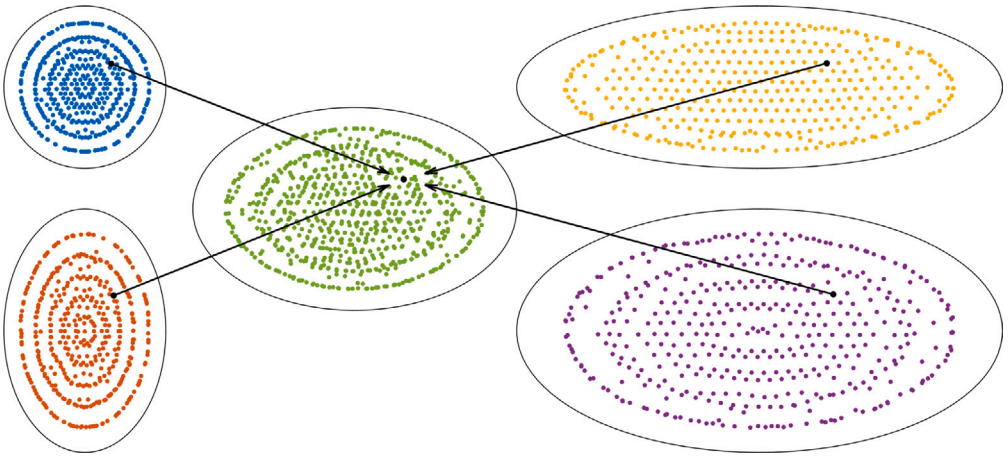

Fig. 17. Set of particles that compose the Gaussian particles decomposition on a new domain (in green). Also, it is represented the "displacement" of the matched particles to the new domain.

geometric parameters space may be separable into L number of degrees of freedom, ψ_m^q can be linearly decomposed in a chosen base N_l^q with the associated coefficients $a_{m,l}^q$:

$$\psi_{i,m}^q(\alpha_q) = \sum_{l=1}^{L} N_l^q(\alpha_q) \cdot a_{i,m,l}^q. \tag{26}$$

where the coefficients $a_{i,m,l}^q$ are the result of a minimization problem. This problem tries to reduce the discrepancy between the POD coefficients and their approximation:

$$\min_{a_{i,m,l}^q} \|\theta_{i,r} - \hat{\theta}_{i,r}\|^2. \tag{27}$$

After finding the coefficients $a_{i,m,l}^q$, we can evaluate the sPGD approximation $\hat{\theta}_{i,r}$ for any value of the geometrical parameters. Fig. 16 shows the values of the 3 first modes of $\hat{\theta}_{i,r}$ by means of the geometric parameters, which are the horizontal l_h and vertical l_v semi-axes of the ellipse.

The previous construction of the parametric model is the last step of the off-line stage. Now, one can explore the space of geometric parameters and get the interpolated parametric solution over a new geometrical domain. Indeed, the parametric model provides the location of the N particles $\mu_i^{\hat{\xi}}$ for a set of new geometrical parameters $(\hat{l}_h, \hat{l}_v)$ in an online manner:

$$\mu_i^{\hat{\xi}} = \hat{\theta}_{i,r}(\alpha_1, \ldots, \alpha_q, \ldots, \alpha_Q) \cdot U_{i,r}. \tag{28}$$

Fig. 17 shows the results of this procedure when applied to a new set of semi-axis, in particular the geometric domain is defined as $\Omega_{x,y} = (2, 1.25)$,while the new set of particles are obtained as $\mu_i^{\hat{\xi}} = \hat{\theta}_{i,r}(2, 1.5) \cdot U_{i,r}$

The sum of the Gaussian functions associated with each particle will provide the spatial PGD mode corresponding with the new domain. Each mode must be then weighted regarding the mode associated with the thermal diffusivity κ. Finally, we sum the contribution of each mode to recover the parametric, as represented in 18. This Figure illustrates the reference temperature field (top) and the recovered one (bottom) for three different values of the thermal diffusivity ($\kappa_{\text{left}} = 1$, $\kappa_{\text{middle}} = 1.5$, and $\kappa_{\text{right}} = 2$).

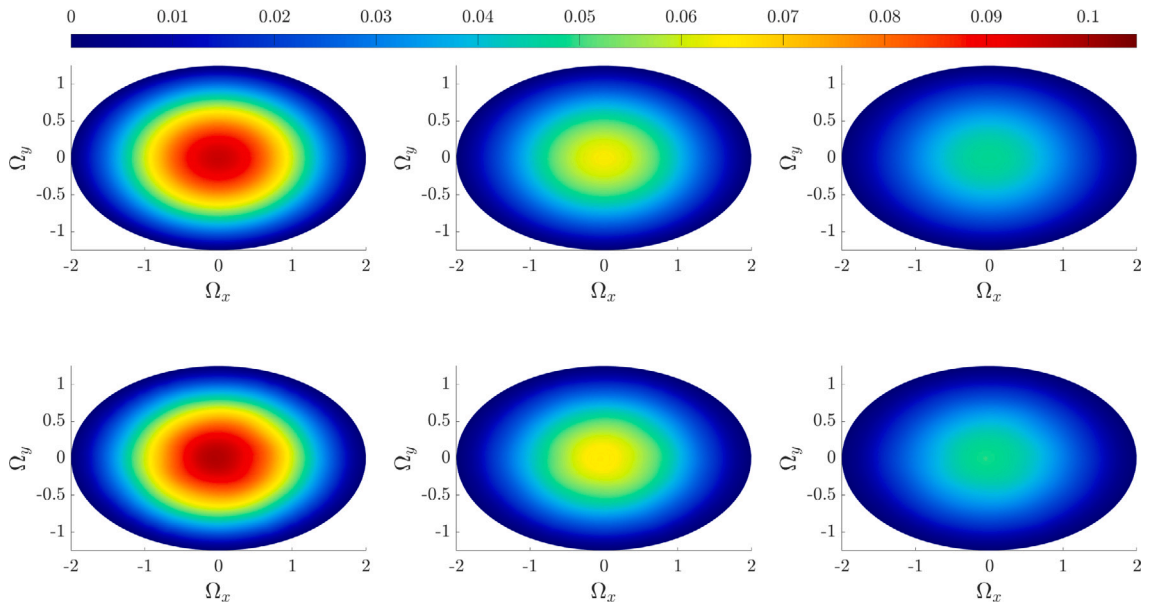

Fig. 18. The temperature field over the domain $\Omega_{x,y} = (2, 1.25)$ is considered, taking into account three different thermal diffusivity values: $\kappa_{\text{left}} = 1$, $\kappa_{\text{middle}} = 1.5$, and $\kappa_{\text{right}} = 2$. The reference solution is shown on top, while the recovered solution obtained through the proposed methodology is illustrated on the bottom.

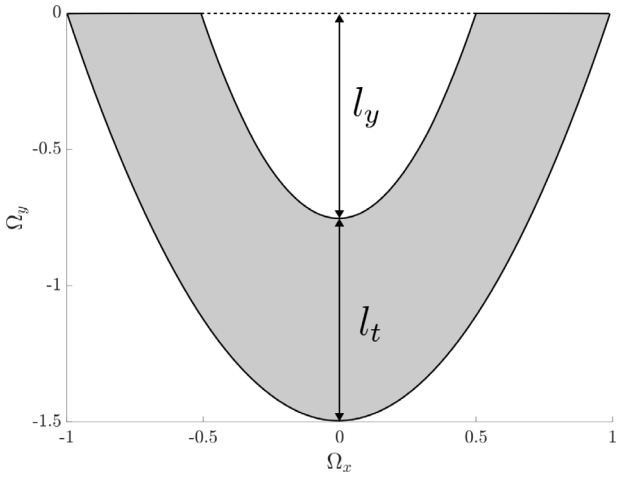

Fig. 19. Geometric domain with the corresponding geometrical parameters: l_y and l_t.

3.3. Non-convex parametric 2D problem

Building upon the rationale demonstrated in the previous example, our objective is to showcase the applicability of the proposed methodology in a non-convex geometrical domain. We will address the steady-state heat Eq. (15), which involves thermal diffusivity parameterized through the PGD framework, much like in the prior example. Let κ symbolize the thermal diffusivity, serving as an additional coordinate within the PGD framework. Its definition spans over the interval $\Omega_\kappa = (1, 2)$, thereby extending the problem domain. The temperature field, denoted as T, is constrained to have a value of 0 along the Dirichlet boundaries Γ_D. The source term $f(x, y)$ is characterized by a bivariate Gaussian function, specifically: $f(x, y) = G_{[\mu_x,\mu_y],[\sigma_x,\sigma_y]}$. Regarding the geometrical domain, we adopt a "U"-like shape, with its parameters measured along the symmetry axis as illustrated in Fig. 19. Consequently, these two length parameters define the geometrical domain as $\Omega_{x,y} = (l_y, l_t)$.

In Fig. 20, we depict four distinct geometric domains utilized to explore the parameter space, characterized by the following coordinates: $\Omega^1_{x,y} = (0.5, 0.5)$, $\Omega^2_{x,y} = (0.5, 1)$, $\Omega^3_{x,y} = (1, 0.5)$, and $\Omega^4_{x,y} = (1, 1)$. Within each of these domains, we showcase a specific solution corresponding to a thermal diffusivity value of $\kappa = 1$. These solutions are associated with the respective source terms defined as follows: $G^1_{[0,-0.75],[0.5,0.25]}$, $G^2_{[0,-1.25],[0.5,0.5]}$, $G^3_{[0,-1],[0.5,0.25]}$, and $G^4_{[0,-1.5],[0.5,0.5]}$.

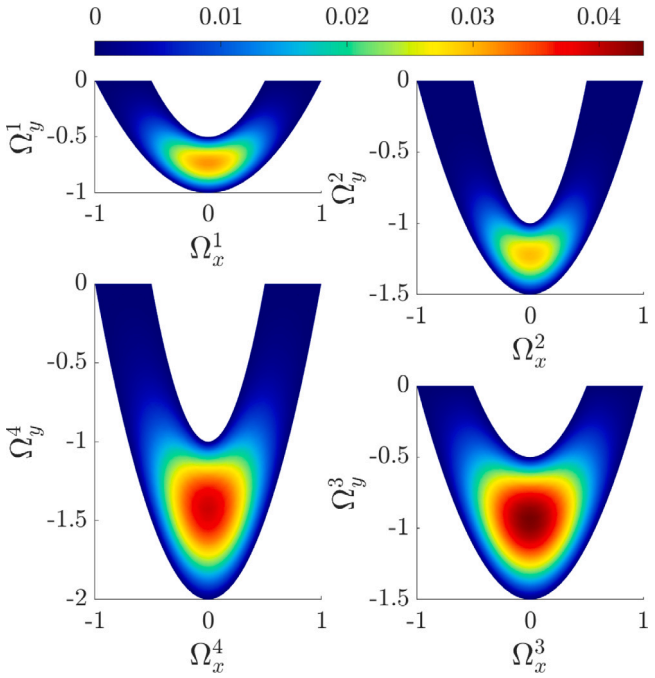

Fig. 20. Sampling of the space of geometrical parameters that contains four individuals. Each spatial domain is illustrated with its corresponding temperature field considering a value of $\kappa = 1$.

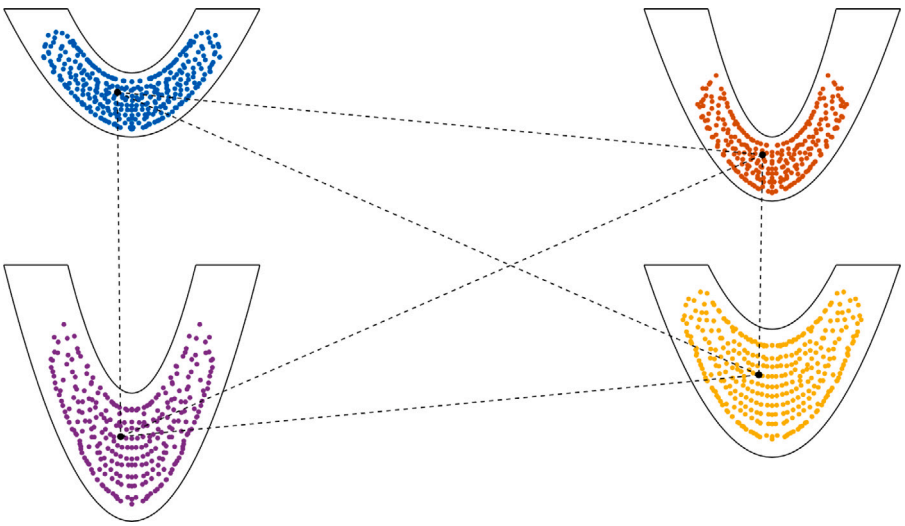

Fig. 21. Particle-based decomposition for each distribution. Also, for one particle, is represented the segments that correspond with the optimal matching.

Particle decomposition. In the context of particle decomposition for each PGD mode, we employ the same approach as demonstrated in the previous example. This entails solving the minimization problem described in (17). Fig. 21 provides a visual representation of the particle set used to reconstruct the first PGD mode in each solution.

Particle matching. In line with our methodology, once we have acquired the particle-based decomposition for each PGD mode, the next step involves the optimal matching of particles within each distribution. This optimization is achieved by minimizing the cost, as defined in (21), using a GA strategy. For a visual representation, Fig. 21 illustrates the particles within each geometrical domain, including a sampled particle and its corresponding matched particles.

Parametric model. The development of the parametric model involves establishing a mapping that can determine particle locations for specific sets of geometric parameters. This process leverages a combination of POD and sPGD. Firstly, POD reduces the particle

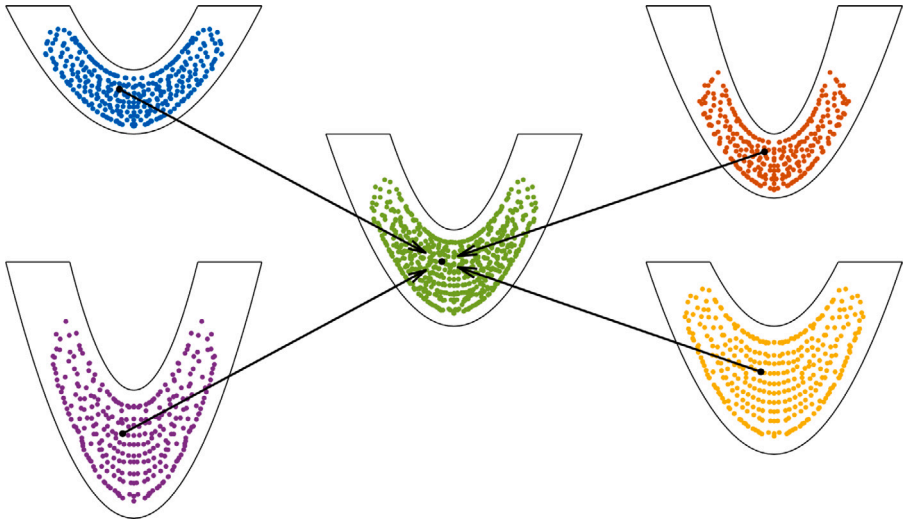

Fig. 22. Set of particles that compose the Gaussian particles decomposition on a new domain (in green). Also, it is represented the "displacement" of the matched particles to the new domain.

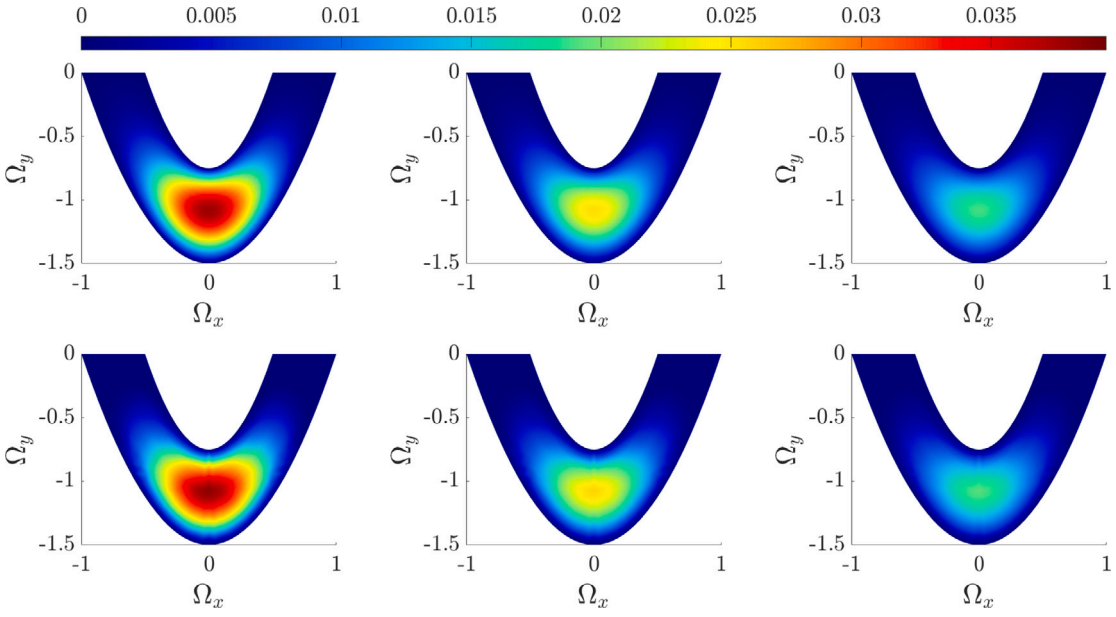

Fig. 23. The temperature field over the domain $\Omega_{x,y} = (0.75, 0.75)$ is considered, taking into account three different thermal diffusivity values: $\kappa_{\text{left}} = 1$, $\kappa_{\text{middle}} = 1.5$, and $\kappa_{\text{right}} = 2$. The reference solution is shown on top, while the recovered solution obtained through the proposed methodology is illustrated on the bottom.

coordinates to a more manageable space. Subsequently, sPGD derives the mapping between the geometric parameters and the reduced space obtained through POD.

Once the parametric model is constructed, it allows for exploration within the space of geometric parameters, facilitating the computation of transported parametric solutions for various geometric domains. For instance, Fig. 22 visually depicts particle locations within the geometric space defined as $\Omega_{x,y} = (0.75, 0.75)$.

Following this, the summation of Gaussian functions associated with each particle serves to reconstruct one of the spatial PGD modes. This process must be iterated for each mode, with subsequent weighting according to the modes related to thermal diffusivity κ. Ultimately, the contribution of each mode combines to yield the sought-after solution. Fig. 23 provides a visual representation of the reference temperature field (top) and the corresponding reconstructed field (bottom) for three distinct values of thermal diffusivity ($\kappa_{\text{left}} = 1$, $\kappa_{\text{middle}} = 1.5$, and $\kappa_{\text{right}} = 2$).

4. Conclusions

In this paper we proposed an OT-PGD approach to transport parametric PGD model known on some geometrical reference domains to intermediate domains. For this, we simplify the Optimal Transport Monge's problem to an optimal deterministic assignment using a particle description of the transported mode. On the simple 1D example and the somehow more elaborate 2D example the use of OT seems to be a very efficient way to transport the mode. The condition of such a successful transport have now to be investigated in order to be able to ensure the condition of a robust an efficient transportation.

The main interest of the approach relies on the possibility to treat of line families of geometries as well as other parameters (material, loading) and provide an attractive tool to explore the parametric space of geometrical parameters and others under tight time constraints. In the future, we would like aim to transport, from an OT point of view, distributions defined by level-sets, which will require a more sophisticated approach.

Furthermore, we are currently focused on implementing the proposed strategy in engineering applications. In this domain, attaining precise accuracy is of utmost importance. It is essential to establish a precise definition for measuring the incurred errors. Additionally, the development of real-time tools holds significant significance in this field. We believe that our proposed strategy can make a valuable contribution towards achieving this objective.

CRediT authorship contribution statement

D. Muñoz: Conceptualization, Methodology, Software, Validation, Formal analysis, Investigation, Data curation, Writing – original draft. **S. Torregrosa:** Conceptualization, Methodology, Software, Writing – review & editing. **O. Allix:** Conceptualization, Methodology, Writing – review & editing. **F. Chinesta:** Conceptualization, Methodology, Writing – review & editing, Funding acquisition.

Declaration of competing interest

The authors declare that they have no known competing financial interests or personal relationships that could have appeared to influence the work reported in this paper.

Data availability

Data will be made available on request.

Acknowledgments

The authors gratefully acknowledge the financial support of the french ANDRA agency, ESI Group through the CREATE-ID chair at Arts et Métiers and the DesCartes programme, supported by the National Research Foundation, Prime Minister's Office, Singapore under its Campus for Research Excellence and Technological Enterprise (CREATE) programme.

References

[1] A. Chatterjee, An introduction to the proper orthogonal decomposition, Current Sci. 78 (2000) 808–817.
[2] G. Berkooz, P. Holmes, J.L. Lumley, The proper orthogonal decomposition in the analysis of turbulent flows 25, 25, 2003, pp. 539–575, http://dx.doi.org/10.1146/ANNUREV.FL.25.010193.002543.
[3] G. Rozza, D.B. Huynh, A.T. Patera, Reduced basis approximation and a posteriori error estimation for affinely parametrized elliptic coercive partial differential equations: Application to transport and continuum mechanics, Arch. Comput. Methods Eng. 15 (2008) 229–275.
[4] B. Schölkopf, A. Smola, K.R. Müller, Nonlinear component analysis as a kernel eigenvalue problem, Neural Comput. 10 (1998) 1299–1319.
[5] H. Hoffmann, Kernel PCA for novelty detection, Pattern Recognit. 40 (2007) 863–874.
[6] I.T. Jolliffe, Principal Component Analysis, Springer-Verlag, New York, 2002.
[7] I.T. Jolliffe, J. Cadima, Principal component analysis: a review and recent developments, Phil. Trans. R. Soc. A 374 (2016).
[8] L. Saul, S. Roweis, An introduction to locally linear embedding, 2001.
[9] B.G. Bghojogh, A.G. Alighodsi, F.K. Karray, M.C. Mcrowley, Locally linear embedding and its variants: Tutorial and survey, 2020.
[10] I. Goodfellow, Y. Bengio, A. Courville, Deep Learning, MIT Press, 2016.
[11] M.A. Kramer, Nonlinear principal component analysis using autoassociative neural networks, AIChE J. 37 (1991) 233–243.
[12] M. Kramer, Autoassociative neural networks, Comput. Chem. Eng. 16 (1992) 313–328.
[13] D.P. Kingma, M. Welling, An introduction to variational autoencoders, Found. Trends Mach. Learn. 12 (2019) 307–392.
[14] Q. Kong, A. Chiang, A.C. Aguiar, M.G. Fernández-Godino, S.C. Myers, D.D. Lucas, Deep convolutional autoencoders as generic feature extractors in seismological applications, Artif. Intell. Geosci. 2 (2021) 96–106.
[15] A. Radford, L. Metz, S. Chintala, Unsupervised representation learning with deep convolutional generative adversarial networks, in: 4th International Conference on Learning Representations, ICLR 2016 - Conference Track Proceedings, in: International Conference on Learning Representations, ICLR, 2015.
[16] A. Ammar, B. Mokdad, F. Chinesta, R. Keunings, A new family of solvers for some classes of multidimensional partial differential equations encountered in kinetic theory modeling of complex fluids, J. Non-Newton. Fluid Mech. 139 (2006) 153–176.
[17] F. Chinesta, R. Keunings, A. Leygue, The Proper Generalized Decomposition for Advanced Numerical Simulations: A Primer, p. 117.
[18] E. Cueto, D. González, I. Alfaro, Proper Generalized Decompositions, Springer International Publishing, Cham, 2016.
[19] M.J. Kazemzadeh-Parsi, A. Ammar, F. Chinesta, Domain decomposition involving subdomain separable space representations for solving parametric problems in complex geometries, Adv. Model. Simul. Eng. Sci. 9 (2022) 1–24.

[20] C. Villani, Optimal Transport, Vol. 338, Springer Berlin Heidelberg, Berlin, Heidelberg, 2009.
[21] G. Monge, M{é}moire sur la th{é}orie des d{é}blais et des remblais, Mem. Math. Phys. Acad. Royale Sci. (1781) 666–704.
[22] L.V. Kantorovich, On the translocation of masses, J. Math. Sci. 133 (2006) 1381–1382.
[23] C. Villani, Topics in Optimal Transportation, p. 378.
[24] L. Vaserstein, Markov processes over denumerable products of spaces, describing large systems of automata, Probl. Pereda. Inf. 5 (1969) 64–72.
[25] B. Engquist, B.D. Froese, Y. Yang, Optimal transport for seismic full waveform inversion, 2016.
[26] L. Métivier, R. Brossier, Q. Mérigot, E. Oudet, J. Virieux, Measuring the misfit between seismograms using an optimal transport distance: application to full waveform inversion, Geophys. J. Int. 205 (1) (2016) 345–377.
[27] J. Solomon, F.D. Goes, G. Peyré, M. Cuturi, A. Butscher, A. Nguyen, T. Du, L. Guibas, Convolutional wasserstein distances, ACM Trans. Graph. 34 (2015).
[28] G. Peyré, M. Cuturi, Computational optimal transport, Found. Trends Mach. Learn. 11 (2018) 1–257.
[29] G. Peyré, M. Cuturi, Computational optimal transport: With applications to data science, Found. Trends Mach. Learn. 11 (2019) 355–607.
[30] C.A. Alfaro, S.L. Perez, C.E. Valencia, M.C. Vargas, The assignment problem revisited, Optim. Lett. 16 (2022) 1531–1548.
[31] S. Torregrosa, V. Champaney, A. Ammar, V. Herbert, F. Chinesta, Surrogate parametric metamodel based on optimal transport, Math. Comput. Simulation 194 (2022) 36–63.
[32] D.J. Price, Smoothed particle hydrodynamics: Things I wish my mother taught me, 2011.
[33] S. Adami, Modeling and simulation of multiphase phenomena with smoothed particle hydrodynamics, 2014.
[34] D. Whitley, A genetic algorithm tutorial, Stat. Comput. 4 (1994) 65–85.
[35] L.M. Schmitt, Theory of genetic algorithms, Theoret. Comput. Sci. 259 (2001) 1–61.
[36] L.M. Schmitt, Theory of genetic algorithms II: models for genetic operators over the string-tensor representation of populations and convergence to global optima for arbitrary fitness function under scaling, Theoret. Comput. Sci. 310 (2004) 181–231.
[37] R.I. nez, E. Abisset-Chavanne, A. Ammar, D. González, E. Cueto, A. Huerta, J.L. Duval, F. Chinesta, A multidimensional data-driven sparse identification technique: The sparse proper generalized decomposition, Complexity 2018 (2018).